25. Kuroiwa Y (1985) Neuromyelitis optica (Devic's disease, Devic's syndrome. In: *Handbook of Clinical Neurology Vol. 3: Demyelinating Diseases*, JC Koetsier (ed.), pp. 397–408. Elsevier Science Publishers: Amsterdam.
26. Lassmann H, Raine CS, Antel J, Prineas JW (1998) Immunopathology of multiple sclerosis: report on an international meeting held at the Institute of Neurology of the University of Vienna. *J Neuroimmunol* **86**:213–217.
27. Lee TS, Eid T, Mane S, Kim JH, Spencer DD, Ottersen OP, de Lanerolle NC (2004) Aquaporin-4 is increased in the sclerotic hippocampus in human temporal lobe epilepsy. *Acta Neuropathol* **108**:493–502.
28. Lennon VA, Wingerchuk DM, Kryzer TJ, Pittock SJ, Lucchinetti CF, Fujihara K *et al* (2004) A serum autoantibody marker of neuromyelitis optica: distinction from multiple sclerosis. *Lancet* **364**:2106–2112.
29. Lennon VA, Kryzer TJ, Pittock SJ, Verkman AS, Hinson SR (2005) IgG marker of optic-spinal multiple sclerosis binds to the aquaporin-4 water channel. *J Exp Med* **202**:473–477.
30. Lucchinetti CF, Mandler RN, McGavern D, Bruck W, Gleich G, Ransohoff RM *et al* (2002) A role for humoral mechanisms in the pathogenesis of Devic's neuromyelitis optica. *Brain* **125**:1450–1461.
31. Matsuoka T, Matsushita T, Kawano Y, Osoegawa M, Ochi H, Ishizu T *et al* (2007) Heterogeneity of aquaporin-4 autoimmunity and spinal cord lesions in multiple sclerosis in Japanese. *Brain* **130**:1206–1223.
32. Matsuoka T, Matsushita T, Osoegawa M, Ochi H, Kawano Y, Mihara F *et al* (2008) Heterogeneity and continuum of multiple sclerosis in Japanese according to magnetic resonance imaging findings. *J Neurol Sci* **266**:115–125.
33. Matsuoka T, Suzuki SO, Iwaki T, Tabira T, Ordinario AT, Kira J (2010) Aquaporin-4 astrocytopathy in Baló's disease. *Acta Neuropathol* **120**:651–660.
34. Matsushita T, Isobe N, Matsuoka T, Ishizu T, Kawano Y, Yoshiura T *et al* (2009) Extensive vasogenic edema of anti-aquaporin-4 antibody-related brain lesions. *Mult Scler* **15**:1113–1117.
35. Matsushita T, Isobe N, Matsuoka T, Shi N, Kawano Y, Wu XM *et al* (2009) Aquaporin-4 autoimmune syndrome and anti-aquaporin-4 antibody-negative opticospinal multiple sclerosis in Japanese. *Mult Scler* **15**:834–847.
36. Matsushita T, Isobe N, Piao H, Matsuoka T, Ishizu T, Doi H *et al* (2010) Reappraisal of brain MRI features in patients with multiple sclerosis and neuromyelitis optica according to anti-aquaporin-4 antibody status. *J Neurol Sci* **291**:37–43.
37. Minohara M, Matsuoka T, Li W, Osoegawa M, Ishizu T, Ohyagi Y, Kira J (2006) Upregulation of myeloperoxidase in patients with opticospinal multiple sclerosis: positive correlation with disease severity. *J Neuroimmunol* **178**:156–160.
38. Misu T, Fujihara K, Kakita A, Konno H, Nakamura M, Watanabe S *et al* (2007) Loss of aquaporin 4 in lesions of neuromyelitis optica: distinction from multiple sclerosis. *Brain* **130**:1224–1234.
39. Nakashima I, Fujihara K, Miyazawa I, Misu T, Narikawa K, Nakamura M *et al* (2006) Clinical and MRI features of Japanese patients with multiple sclerosis positive for NMO-IgG. *J Neurol Neurosurg Psychiatry* **77**:1073–1075.
40. Okinaka S, Tsubaki T, Kuroiwa Y, Toyokura Y, Imamura Y (1958) Multiple sclerosis and allied diseases in Japan; clinical characteristics. *Neurology* **8**:756–763.
41. Osoegawa M, Kira J, Fukazawa T, Fujihara K, Kikuchi S, Matsui M *et al* (2009) Temporal changes and geographical differences in multiple sclerosis phenotypes in Japanese: nationwide survey results over 30 years. *Mult Scler* **15**:159–173.
42. Paul F, Jarius S, Aktas O, Bluthner M, Bauer O, Appelhans H *et al* (2007) Antibody to aquaporin 4 in the diagnosis of neuromyelitis optica. *PLoS Med* **4**:e133.
43. Pittock SJ, Lennon VA, Krecke K, Wingerchuk DM, Lucchinetti CF, Weinshenker BG (2006) Brain abnormalities in neuromyelitis optica. *Arch Neurol* **63**:390–396.
44. Poser CM, Paty DW, Scheinberg L, McDonald WI, Davis FA, Ebers GC *et al* (1983) New diagnostic criteria for multiple sclerosis: guidelines for research protocols. *Ann Neurol* **13**:227–231.
45. Roemer SF, Parisi JE, Lennon VA, Benarroch EE, Lassmann H, Bruck W *et al* (2007) Pattern-specific loss of aquaporin-4 immunoreactivity distinguishes neuromyelitis optica from multiple sclerosis. *Brain* **130**:1194–1205.
46. Saadoun S, Waters P, Bell BA, Vincent A, Verkman AS, Papadopoulos MC (2010) Intra-cerebral injection of neuromyelitis optica immunoglobulin G and human complement produces neuromyelitis optica lesions in mice. *Brain* **133**:349–361.
47. Sabater L, Giralt A, Boronat A, Hankiewicz K, Blanco Y, Llufriu S *et al* (2009) Cytotoxic effect of neuromyelitis optica antibody (NMO-IgG) to astrocytes: an *in vitro* study. *J Neuroimmunol* **215**:31–35.
48. Sharma R, Fischer MT, Bauer J, Felts PA, Smith KJ, Misu T *et al* (2010) Inflammation induced by innate immunity in the central nervous system leads to primary astrocyte dysfunction followed by demyelination. *Acta Neuropathol* **120**:223–236.
49. Su JJ, Osoegawa M, Matsuoka T, Minohara M, Tanaka M, Ishizu T *et al* (2006) Upregulation of vascular growth factors in multiple sclerosis: correlation with MRI findings. *J Neurol Sci* **243**:21–30.
50. Tabira T, Tateishi J (1982) Neuropathological features of MS in Japan. In: *Multiple Sclerosis East and West*, Y Kuroiwa, LT Kurland (eds), pp. 273–295. Kyushu University Press: Fukuoka.
51. Viegas S, Weir A, Esiri M, Kuker W, Waters P, Leite MI *et al* (2009) Symptomatic, radiological and pathological involvement of the hypothalamus in neuromyelitis optica. *J Neurol Neurosurg Psychiatry* **80**:679–682.
52. Vincent T, Saikali P, Cayrol R, Roth AD, Bar-Or A, Prat A, Antel JP (2008) Functional consequences of neuromyelitis optica-IgG astrocyte interactions on blood-brain barrier permeability and granulocyte recruitment. *J Immunol* **181**:5730–5737.
53. Wang CD, Zhang KN, Wu XM, Gang H, Xie XF, Qu XH, Xiong YQ (2008) Balo's disease showing benign clinical course and co-existence with multiple sclerosis-like lesions in Chinese. *Mult Scler* **14**:418–424.
54. Wingerchuk DM, Hogancamp WF, O'Brien PC, Weinshenker BG (1999) The clinical course of neuromyelitis optica (Devic's syndrome). *Neurology* **53**:1107–1114.
55. Wingerchuk DM, Lennon VA, Pittock SJ, Lucchinetti CF, Weinshenker BG (2006) Revised diagnostic criteria for neuromyelitis optica. *Neurology* **66**:1485–1489.
56. Wingerchuk DM, Lennon VA, Lucchinetti CF, Pittock SJ, Weinshenker BG (2007) The spectrum of neuromyelitis optica. *Lancet Neurol* **6**:805–815.
57. Yanagawa K, Kawachi I, Toyoshima Y, Yokoseki A, Arakawa M, Hasegawa A *et al* (2009) Pathologic and immunologic profiles of a limited form of neuromyelitis optica with myelitis. *Neurology* **73**:1628–1637.

Neurochem Res (2011) 36:58–66
DOI 10.1007/s11064-010-0263-7

ORIGINAL PAPER

Tissue Binding Patterns and In Vitro Effects of *Campylobacter jejuni* DNA-Binding Protein from Starved Cells

Hua Piao · Motozumi Minohara · Nobutoshi Kawamura · Wei Li · Takuya Matsushita · Ryo Yamasaki · Yoshimitsu Mizunoe · Jun-ichi Kira

Accepted: 3 September 2010 / Published online: 19 September 2010

Abstract *Campylobacter jejuni* (*C. jejuni*) is frequently associated with axonal Guillain-Barré syndrome (GBS). We reported that *C. jejuni* DNA-binding protein from starved cells (C-Dps) binds to and damages myelinated nerves in vivo. We studied the binding patterns of C-Dps to nervous tissues and its in vitro effects on neural cells. Immunohistochemically, C-Dps labeled the nodes of Ranvier, the outermost parts of internodal myelin and the basement membrane in the peripheral nerves, and neurons and myelin in the central nervous tissues. Its binding was blocked by sulfatide. C-Dps bound to the cell surfaces of nerve growth factor (NGF)-treated PC12 cells leading to dose-dependent LDH release, which was inhibited by either heat-denaturation of C-Dps or coincubation with an anti-C-Dps mAb. However, its binding to the surfaces of cultured NSC34 cells, S16 cells, or dorsal root ganglion cells, did not induce cytotoxicity. These findings suggest a possible involvement of C-Dps in *C. jejuni*-related GBS.

Keywords Guillain-Barré syndrome · *Campylobacter jejuni* · DNA-binding protein from starved cells · Axonal degeneration · Node of Ranvier · Sulfatide

Hua Piao and Motozumi Minohara contributed equally to this work.

H. Piao · M. Minohara · N. Kawamura · W. Li · T. Matsushita · R. Yamasaki · J. Kira (✉)
Department of Neurology, Neurological Institute, Graduate School of Medical Sciences, Kyushu University, 3-1-1 Maidashi, Higashi-ku, Fukuoka 812-8582, Japan
e-mail: kira@neuro.med.kyushu-u.ac.jp

Y. Mizunoe
Department of Bacteriology, Jikei University School of Medicine, Tokyo 105-8461, Japan

Introduction

Campylobacter jejuni (*C. jejuni*) enteritis is the most common antecedent to GBS [1]. GBS is primarily considered to be an inflammatory demyelinating neuropathy; however, prominent axonal involvement is frequently seen in GBS patients following *C. jejuni* infection [2]. This is termed acute motor axonal neuropathy [3], or, in the more severe form, acute motor and sensory axonal neuropathy [4]. Electrophysiologically, simple reduction of compound muscle action potentials without conduction delay is characteristic [5, 6]. Although some patients with this condition may initially have prolonged distal latency, this is rapidly normalized, in contrast with the progressive increase in distal latency in patients with demyelinating GBS [5, 6]. Pathologically, Wallerian-like degeneration and infiltration of periaxonal macrophages are prominent features, while demyelination and lymphocytic infiltration are minimal or even lacking [7]. The earliest changes seen include nodal lengthening and paranodal myelin detachment [8], while in some autopsied patients, severe paralysis occurs in the absence of visible changes during an ordinary pathological investigation [7].

In this condition, anti-GM1 ganglioside antibody is hypothesized to be pathogenic through molecular mimicry between human GM1 ganglioside and *C. jejuni* lipo-oligosaccharide [9]. IgG, C3 and membrane attack complex were found to be deposited in the nodes of Ranvier in autopsied patients with axonal GBS [10] and its animal model immunized with a bovine brain ganglioside mixture including GM1 [11]. The frequency of occurrence of anti-GM1 antibodies in GBS patients (10–48%) is at best statistically significant as compared with healthy controls [1, 2, 9, 12, 13]. The reproduction of clinical and pathological components of the disease by passive transfer of anti-GM1 antibodies to experimental animals has been reported [11, 14–16];

however the ability of these antibodies to bind and exert pathogenic effects is inconsistent. Such inconsistency is considered to arise from the local glycolipid microenvironment where GM1 is cryptic [16]. Taking the presence of anti-GM1 antibody-negative axonal GBS cases into account, the role of anti-GM1 antibodies still needs further investigation.

We purified and characterized a DNA-binding protein from starved cells (Dps) derived from *C. jejuni* [17]. The C-Dps protein was found to share 41 and 24% amino acid identities with *Helicobacter pylori* neutrophil-activating protein (HP-NAP) and *Escherichia coli* (*E. coli*) Dps, respectively. These proteins constitute the Dps protein family, are produced at high levels under conditions of oxidative or nutritional stress, and efficiently protect bacterial DNA. HP-NAP lacks DNA binding capability, but through binding to neutrophil glycosphingolipids, such as sulfatide, is chemotactic for human neutrophils [18]. Recently, sulfatide was found to be essential for paranodal junction formation and for the maintenance of ion channels on myelinated axons [19, 20]. These findings prompted us to investigate the effects of C-Dps on myelinated axons and the possible involvement of C-Dps in *C. jejuni*-related GBS, and we recently reported that C-Dps binds to and damages myelinated nerve fibers through binding with sulfatide [21]. In the present study, we examined the binding characteristics of C-Dps to nervous tissues and its in vitro effects on neural cells.

Materials and Methods

Purification of Recombinant C-Dps Protein

E. coli BL21 (DE3) cells harboring the *dps* gene were grown in LB-ampicillin (50 μg/ml) at 37°C overnight. After expression of *dps* was induced with 1 mM isopropyl-D-thiogalactoside for 3 h, bacterial cells were harvested (15,000*g* for 1 h) and resuspended in 20 mM Tris–HCL buffer (pH 8.0). After cell disruption by sonication, the lysates were centrifuged at 4°C (39,000*g* for 20 min). Supernatants containing C-Dps were purified using Ni–NTA agarose columns and dialyzed against PBS-0.1 mM EDTA [17]. Thereafter, endotoxin levels were decreased by affinity chromatography using a polymyxin B agarose gel (Sigma, MO, USA). We assayed the endotoxin level in the final protein solution using a QCL-1000 kit (BioWhittaker, Belgium), and the levels were found to be less than 10 EU/mg.

Immunohistochemistry for C-Dps Binding to Central and Peripheral Nervous Tissues

To study C-Dps binding to central nervous tissues, 8-week-old female Lewis rats were fixed by transcardial perfusion with 4% paraformaldehyde in PBS. Brains and spinal cords were harvested and cut into 10-μm sections. Frozen brain and spinal cord sections were exposed to C-Dps (5 μg/ml) at room temperature for 1 h. Unbound C-Dps was removed by washing sections in 50 mM Tris–HCl (pH 7.6) and bound protein was detected by using an anti-C-Dps mAb (1:200). Control sections were incubated without C-Dps. After washes with Tris–HCl, the sections were incubated at room temperature with HRP-conjugated anti-mouse IgG (1:200) for 1 h. After washing them in Tris–HCl, the slides were dipped in 0.2 mg/ml 3, 3′-diaminobenzidine tetrahydrochloride in PBS containing 0.01% H_2O_2 for 20–30 s, washed in water and dehydrated sequentially in 70, 90% and absolute ethanol for 3 min each, followed by three washes in xylene for 3 min each. Slides were then mounted with EUKITT (O. Kindler, Germany).

To study binding of C-Dps to peripheral nerves, rat sciatic nerves were harvested in the same manner as central nervous system (CNS) tissues, coated in OCT compound (Sakura Finetek, CA, USA) and cut into 10-μm sections in longitudinal and transverse planes. Sections were exposed to 5 μg/ml C-Dps solution at room temperature for 1 h. Unbound C-Dps was removed by washing the sections with Tris–HCl. Control sections were incubated without C-Dps. For double immunostaining, anti-C-Dps mAb (1:200) and rabbit anti-neurofilament 200 kD (NF) polyclonal antibody (1:200) (Chemicon, MA, USA) were applied at room temperature for 1 h followed by incubation with donkey anti-mouse IgG-fluoresceinisothiocyanate (FITC) (1:200) (Jackson ImmunoResearch Laboratories, PA, USA) and goat anti-rabbit IgG-rhodamine (1:200) (Molecular Probes, OR, USA) for 30 min at room temperature. Slides were then washed and mounted in Vectashield (Vector Laboratories). Images were captured by confocal laser scanning microscopy (CLSM, Fluoview FV300, Olympus, Japan).

For immunohistochemistry of teased nerve fibers, rats were perfused through the heart with 2% paraformaldehyde in PBS. The sciatic nerves and the cauda equina were removed and incubated in collagenase type IV in PBS for 20 min at room temperature. After washing, the nerves were de-sheathed and teased into small bundles of fibers under a stereomicroscope. The teased fibers were incubated in blocking buffer (5% goat serum and 1% BSA in PBS) for 15 min. After blocking, they were incubated with biotin-conjugated peanut agglutinin (PNA) (10 μg/ml) (Vector Laboratories), anti-sodium channel Scn8a antibody (1 μg/ml) (Sigma), anti-myelin basic protein (MBP) antibody (1:200) (Acris Antibodies GmbH, Germany), an anti-NF antibody (1:400), or anti-laminin antibody (1:25) (Sigma) in blocking buffer, for 1 h at room temperature. To study C-Dps binding to peripheral nervous tissues, the teased fibers were exposed to C-Dps (5 μg/ml) at room temperature for 1 h and bound protein was detected using an anti-C-Dps mAb (1:5,000). Binding of these antibodies was detected by incubating fibers

with dichlorotriazinyl aminofluorescein (DTAF)-conjugated streptavidin (2 μg/ml) (Immunotech, France), Alexa Fluor 488 anti-mouse IgG (1:1,000) or Alexa Fluor 594 anti-rabbit IgG (1:1,000). Images were captured by CLSM.

Sulfatide blocking of C-Dps binding to myelinated axons was performed as follows. Teased sciatic nerve fibers from Lewis rats were prepared and incubated in blocking buffer for 15 min. After blocking, they were incubated with C-Dps (5 μg/ml) pre-incubated with sulfatide (200 μg/ml), C-Dps (5 μg/ml) pre-incubated with GM2 ganglioside (200 μg/ml) or C-Dps (5 μg/ml) alone, at room temperature for 1 h, and C-Dps binding to teased fibers was detected using an anti-C-Dps mAb (1:5,000) and Alexa Fluor 488 anti-mouse IgG. Images were captured by CLSM.

Cell Cultures

To determine the effects of C-Dps on neuronal cells in vitro, PC12 cells were propagated in RPMI 1640 containing 10% horse serum, 5% FBS, 2 nM L-glutamine, 50 units/ml penicillin, and 50 μg/ml streptomycin (RPMI with serum, abbreviated as M/S) (Gibco). The cells were grown on 12-well collagen-coated microplates (8×10^4 cells/well, Iwaki Asahi TechnoGlass, Japan) for the C-Dps treatment, and on collagen-treated coverslips (1×10^4 cells/coverslip, Iwaki Asahi TechnoGlass, Japan) for imaging by CLSM. The cells were differentiated for up to 6 days in M/S supplemented with 100 ng/ml NGF-7S (Sigma) (abbreviated as M/S + N).

To determine the effects of C-Dps on Schwann cells in vitro, S16 cells [22] were used. Cells were cultured in DMEM containing 10% FBS, 25 units/ml penicillin and 25 μg/ml streptomycin (DMEM with serum, abbreviated as D/S) (Gibco). The cells were grown on 96-well collagen-coated microplates (1.6×10^3 cells/well) for C-Dps treatment, and on collagen-treated coverslips (1×10^3 cells/coverslip) for imaging with CLSM.

The DRG cells of embryonic 15-day-old Wistar rats were plated on culture dishes and cultured at 37°C in a 5% CO_2 incubator in SUMILON Medium/Neuron (containing glial conditioned medium, No. MB-X9501; Sumitomo Bakelite Co. Ltd., Japan). Dissociated DRG cells were cultured for 3 days and treated with 10 μM uridine (Sigma) and 10 μM fluorodeoxyuridine (Sigma) for an additional 3 days.

NSC34 cells, mouse embryonic spinal cord-neuroblastoma cell line cells with a motor neuron phenotype, were grown in D/S at 37°C in the presence of 5% CO_2.

Immunohistochemistry of C-Dps Binding to Cultured Cells

For immunohistochemistry of C-Dps binding to NGF-treated PC12 cells and NSC34 cells, cells grown on coverslips were fixed in 4% paraformaldehyde for 20 min at room temperature and permeabilized with 0.1% Triton X-100. The coverslips were then washed and coated with 1% BSA in PBS and C-Dps (5 μg/ml) was added to the coverslips and incubated for 1 h at room temperature. After washing coverslips with PBST, anti-C-Dps mAb (1:200 on the basis of preliminary experiments) or anti-NF antibody (1:200) (as a control) was added to the coverslips, and either donkey anti-mouse IgG-FITC (1:200) or anti-rabbit IgG-rhodamine (1:200) was added to visualize staining. For immunohistochemistry of C-Dps binding to S16 cells and DRG cells, cells grown on coverslips were fixed in acetone for 5 min and dried. The coverslips were incubated in blocking buffer (5% skim milk powder in TBST) for 15 min. C-Dps (0.5 μg/ml) was then added to the coverslips and incubated for 1 h at room temperature. After washing, the coverslips were incubated with anti-C-Dps mAb (1:5,000 on the basis of preliminary experiments) at room temperature for 1 h followed by incubation with donkey anti-mouse IgG-FITC (1:200) for 30 min.

Cytotoxicity Assay

For PC12 cells, following incubation for 6 days in M/S + N, cells underwent three successive washes in RPMI to remove NGF and serum-borne trophic agents. They were then placed into medium only as a negative control, 1% Triton X-100 in medium as a positive control, or treated with different doses of C-Dps for 1 h at 36.5–37.5°C in a 5% CO_2 homeothermic blanket, and grown on 12-well collagen-coated plates. Cytotoxicity was evaluated at 1 h after the addition of C-Dps (0.04, 0.2, 1, 5 μg/ml) or heat-denatured C-Dps (100°C, 30 min) by measuring lactate dehydrogenase (LDH) release (a marker of cell membrane damage) using an LDH leakage assay kit (TAKARA BIO, Japan). To examine the specificity of C-Dps cytotoxicity, anti-C-Dps mAb (0.5 μg/ml) was added together with C-Dps in several experiments.

For S16 cells, following 6 days of growth in D/S, cells were placed in N2 medium (1:1 mixture of DMEM and Ham's F-12 supplemented with N-2 supplement, Gibco) containing 10% FBS in collagen-coated microplates for 1 day. After 3 days of growth in N2 medium the cells were washed with PBS and had medium added as a negative control, medium containing 1% Triton X-100 added as a positive control, or treated with different doses of C-Dps for 1 or 5 h at 36.5–37.5°C in a 5% CO_2 homeothermic blanket. The cytotoxicity of C-Dps toward S16 cells was evaluated after addition of medium (0.04, 0.2, 1, 5 μg/ml, 1 h) or high doses of C-Dps (0.2, 1, 5, 25 μg/ml, 5 h) using an LDH leakage assay kit (Takara Bio).

For DRG cells and NSC34 cells, cells were grown on 96-well collagen-coated plates for C-Dps treatment. The

cells were washed with PBS and the cytotoxicity of C-Dps was evaluated at 1, 5, and 24 h after the addition of C-Dps (0.04, 0.2, 1, 5, 25 μg/ml) by measuring LDH release.

Results

Binding of C-Dps in Tissue

By double immunostaining using an anti-C-Dps mAb and an anti-NF antibody, C-Dps was found to associate with the outer part of the myelin sheath and localize to the nodal region in rat peripheral nervous system (PNS) tissues (Fig. 1a). Within the grey matter of the CNS, C-Dps binding was predominantly seen on neurons in the anterior horns of the spinal cord (Fig. 1b) and in the cerebral cortex (Fig. 1c), but it was also seen on myelin within CNS white matter (Fig. 1d). Immunostaining of teased fibers from PNS tissue with an anti-C-Dps mAb and an anti-NF antibody revealed that C-Dps labels the outermost parts of internodal myelin and the nodes of Ranvier (Fig. 2a). The binding pattern of C-Dps was the same as that of PNA, as shown by double immunostaining with PNA and an anti-NF antibody (Fig. 2b). This was further confirmed by double immunostaining for C-Dps and MBP (Fig. 2c). However, double immunostaining with anti-laminin antibody and anti-C-Dps mAb following exposure to C-Dps revealed that C-Dps was also colocalized with laminin in the teased fibers (Fig. 2d–f). Preincubation of C-Dps with sulfatide (sulfatide blocking) markedly attenuated its binding to teased nerve fibers compared with that of C-Dps alone (Fig. 2g, h). C-Dps preincubated with the GM2 ganglioside bound to teased fibers as efficiently as C-Dps alone (Fig. 2i).

In Vitro Effects of C-Dps on Cultured Neuronal and Schwann Cells

We then examined the effects of C-Dps on cultured neuronal cells and Schwann cells in vitro. C-Dps bound to the

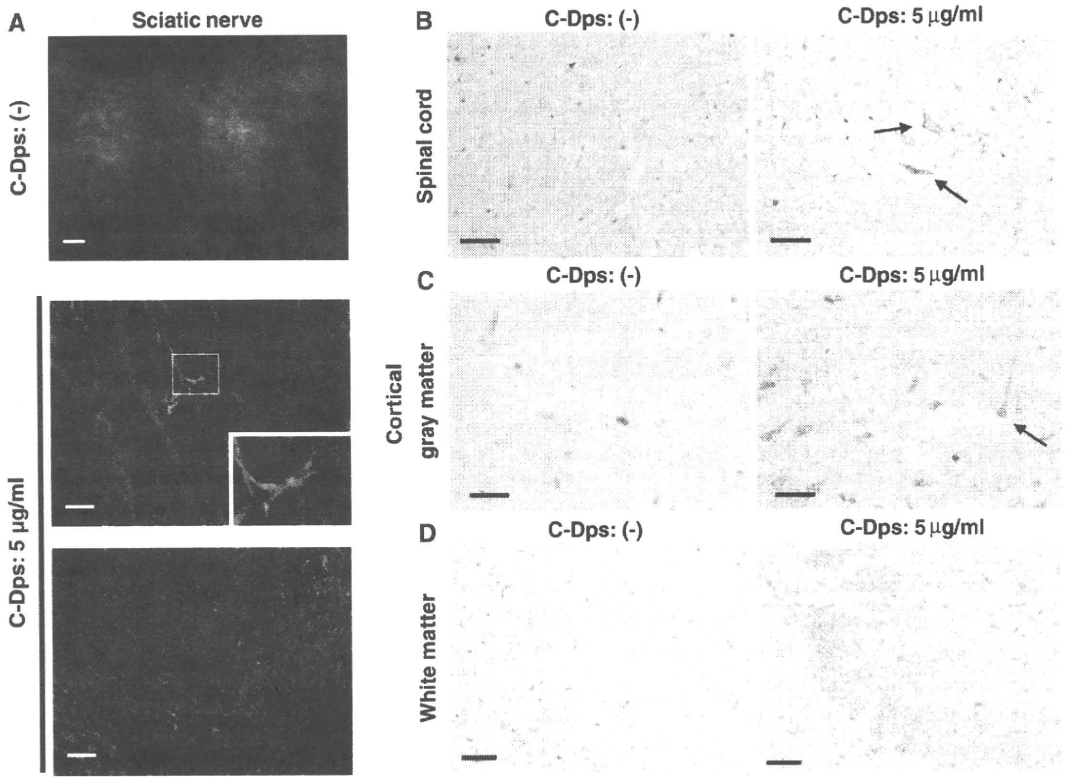

Fig. 1 C-Dps binds to the anterior horn cells in the spinal cord grey matter and neurons in the cerebral cortex, and stains myelin in the white matter. **a** Rat sciatic nerve sections were exposed to C-Dps and stained with anti-C-Dps mAb (*green*) and polyclonal anti-neurofilament IgG (*red*). C-Dps immunostains the outer part of myelin and the nodal regions (*inset*: higher magnification). **b** In the grey matter of the rat spinal cord, C-Dps predominantly stains neurons (*arrow*) in the anterior horns. Control sections were stained in the absence of C-Dps protein. **c** In the rat cerebral cortex, C-Dps mainly stains neurons (*arrow*). **d** In the white matter of the cerebrum, myelin is mainly stained with C-Dps. *Scale bars* in **a** = 10 μm, **b** = 20 μm, **c** = 20 μm, **d** = 50 μm. C-Dps = *Campylobacter jejuni* DNA-binding protein from starved cells. For interpretation of the references to color in this figure legend, the reader is referred to the online version of this article

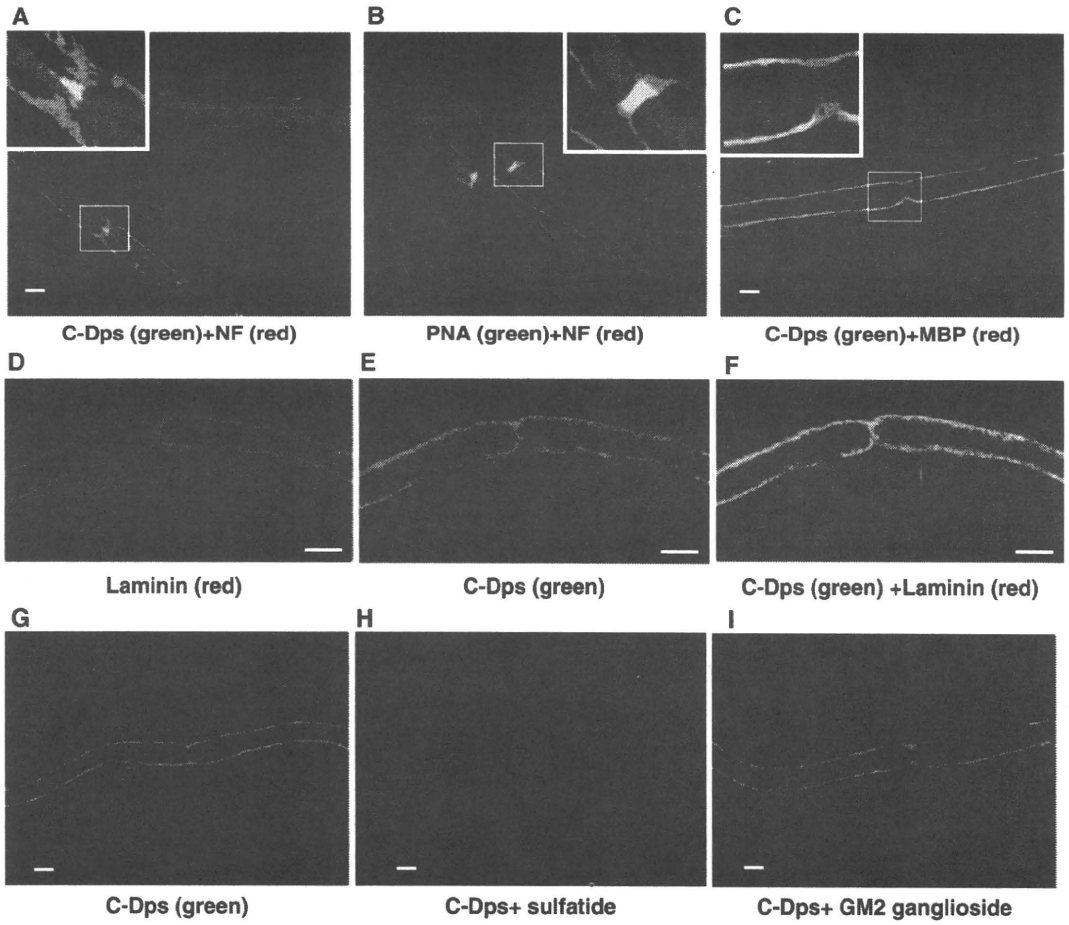

Fig. 2 C-Dps binds to the outermost part of the myelin sheath and the nodes of Ranvier in peripheral nerves. **a** Double immunostaining of teased nerve fibers with anti-neurofilament (NF) antibody (*red*) and with C-Dps followed by anti-C-Dps mAb (*green*). **b** Double immunostaining of teased nerve fibers with anti-NF antibody and with peanut agglutinin (PNA) (*green*). **c** Double immunostaining of teased nerve fibers with anti-MBP antibody (*red*) and with C-Dps followed by anti-C-Dps mAb (*green*). **d** Immunostaining of teased nerve fibers with anti-laminin antibody (*red*). **e** Immunostaining of teased nerve fibers with C-Dps followed by anti-C-Dps mAb (*green*). **f** Double immunostaining of teased nerve fibers with anti-laminin antibody (*red*) and with C-Dps followed by anti-C-Dps mAb (*green*). **g** Immunostaining with anti-C-Dps antibody of teased nerve fibers exposed to C-Dps alone. **h** C-Dps pre-incubated with sulfatide. **i** C-Dps pre-incubated with GM2 ganglioside. *Insets* higher magnification. *Scale bars* 10 μm. C-Dps = *Campylobacter jejuni* DNA-binding protein from starved cells. For interpretation of the references to color in this figure legend, the reader is referred to the online version of this article

cell surfaces of NGF-treated PC12 cells (Fig. 3a). Incubation with C-Dps for 1 h dose-dependently induced LDH release into the supernatant (Fig. 3b). The LDH release from these cells was inhibited by either heat-denaturation of C-Dps or coincubation with an anti-C-Dps mAb (Fig. 3c, d). C-Dps also bound to cultured cells of a Schwann cell line, S16, in vitro (Fig. 3e), but LDH release from these cells was not observed following incubation with C-Dps, even at a higher doses (up to 25 μg/ml), or following longer incubation times (up to 5 h) (Fig. 3f, g). We also examined the effects of C-Dps on DRG cells and NSC34 cells in vitro. C-Dps bound to the surfaces of DRG cells (Fig. 3h) and NSC34 cells (Fig. 3j); however, incubation with C-Dps at a higher doses (up to 25 μg/ml) for 1 h did not induce LDH release from either DRG cells or NSC34 cells (Fig. 3i, k). In NSC34 cells, longer incubation time of up to 24 h with C-Dps (25 μg/ml) did not induce a significant increase in LDH release.

Discussion

The present study revealed that, in tissue, C-Dps binds to not only the nodes of Ranvier, the outermost parts of internodal myelin and the basement membrane in the peripheral nerves, but also the anterior horn cells in the

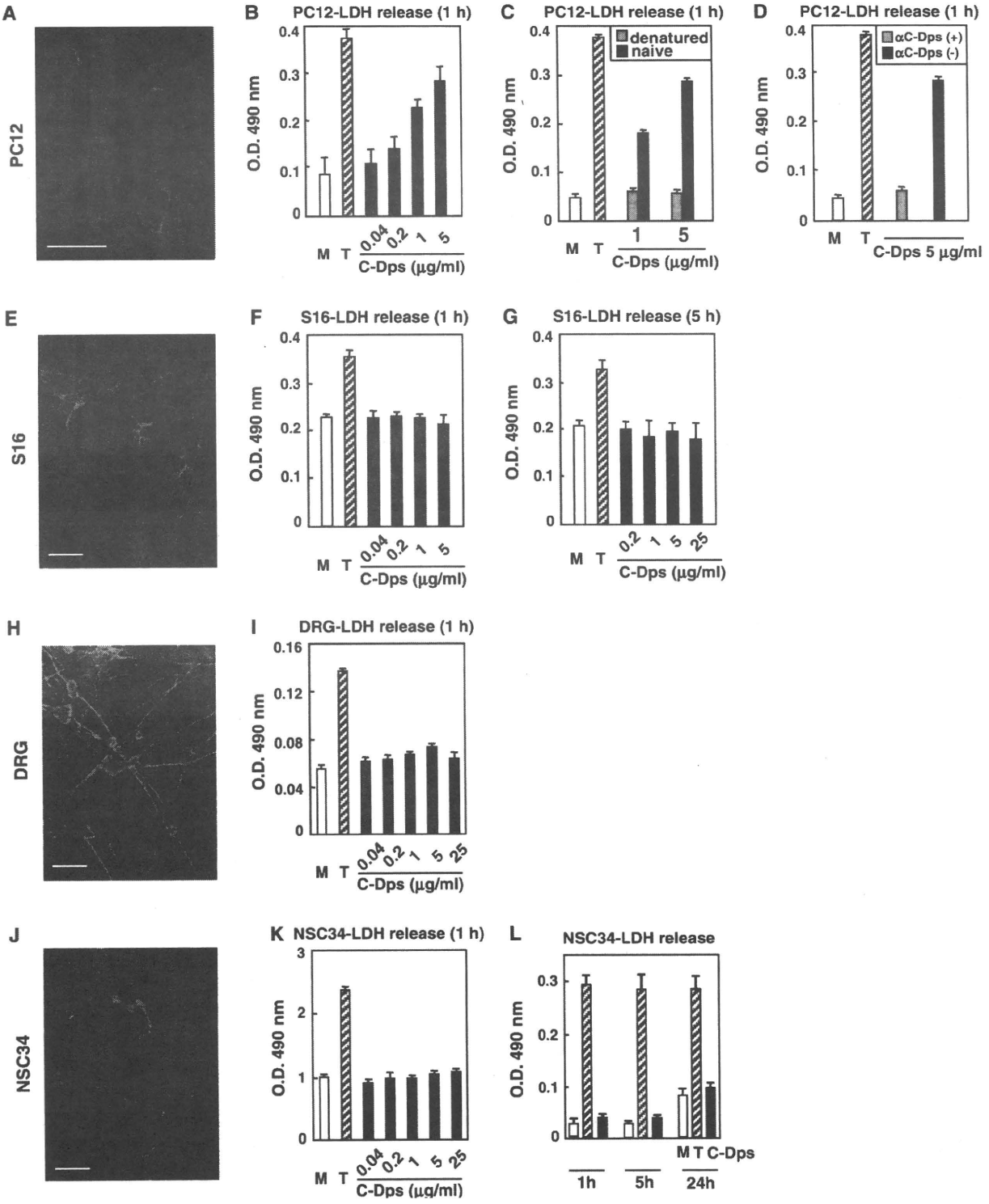

spinal cord grey matter, neurons in the cerebral cortex, and myelin in the white matter. It also revealed that, in culture, C-Dps bound to the cell surfaces of NGF-treated PC12 cells dose-dependently damages these cells, whereas its binding to the surfaces of cultured NSC34 cells, S16 cells, or dorsal root ganglion cells, did not induce cytotoxicity, even at a higher dose and with longer exposure time.

◀ **Fig. 3** **a** C-Dps binds to the cell surface of NGF-treated PC12 cells. **b** C-Dps dose-dependently induces LDH release from NGF-treated PC12 cells. **c** LDH release from PC12 cells is abolished when using heat-denatured C-Dps (100°C, 30 min). **d** Coincubation with anti-C-Dps mAb blocks its effects on PC12 cells. **e** C-Dps binds to the immortalized Schwann cell line, S16 cells. **F**, **G** LDH release is not evident following incubation with C-Dps from Schwann cells, even at higher doses (up to 25 μg/ml) and with longer incubation times (up to 5 h). **h** Binding of C-Dps to DRG cells. **i** LDH release is not evident following incubation with C-Dps from DRG cells. **j** Binding of C-Dps to NSC34 cells. **k** LDH release is not seen following incubation with higher doses of C-Dps (up to 25 μg/ml). **h** LDH release from NSC34 cells is not evident even after longer incubation time (up to 24 h) with C-Dps. *Error bars* indicate means ± SD. *DRG* dorsal root ganglion cells, *M* medium alone, *T* Triton X-100, *αC-Dps* anti-C-Dps monoclonal antibody. *Scale bar* 40 μm

We recently reported that C-Dps induces paranodal myelin detachment and axonal degeneration in vivo [21]. To clarify the mechanisms of action of C-Dps, in the present study we investigated the in vitro effects of C-Dps in various neuronal cells and Schwann cells. In culture, C-Dps induced dose-dependent LDH release from NGF-treated PC12 cells. However, no direct toxicity against either NSC34 motor neuron-like cell line cells or cultured DRG cells was observed, despite C-Dps binding to the surfaces of all of these cell types. Although the reason for this discrepancy is unknown at present, the neurotoxic effects of C-Dps appear to be limited to some neuronal cells. Therefore, it is still possible that C-Dps may cause direct nodal axolemmal damage, or, alternatively, that it may interfere with the functions of sulfatide in the peripheral nerves, even though C-Dps does not directly cause Schwann cell damage. Supporting the latter possibility, cerebroside sulphotransferase knock-out mice, which have a selective sulfatide deficiency, show disruption of paranodes without demyelination of internodal myelin [19, 20]. In this model, sodium channels cluster normally during development, but clustering decreases with age leading to disorganization of the paranodal structure, and sulfatide is considered to be essential for the maintenance of paranodes [19, 20]. It is thus possible that C-Dps may interfere with the functions of paranodal sulfatide, resulting in myelin detachment and unclustering of sodium channels. Second, sulfatide is essential for anchoring the basal lamina to the Schwann cell abaxonal membrane through binding to laminin [23]. Because disruption of the anchoring between the basal lamina and Schwann cells can induce down-modulation of nodal sodium channels [24], C-Dps may also induce nodal sodium channel dysfunction through interfering with the interaction between laminin on the basal lamina and sulfatide on the Schwann cell abaxonal membrane.

In either case, because the effects of C-Dps are efficiently blocked by the addition of an anti-C-Dps antibody in culture, the anti-C-Dps antibody may act protectively in vivo in patients with *C. jejuni*-related GBS. Alternatively, because Wirguin et al. [25] demonstrated that the presence of anti-cholera toxin antibody exacerbated axonal degeneration induced by intraneurally injected cholera toxin, C-Dps combined with anti-C-Dps antibody may worsen the motor neuropathy in patients with *C. jejuni*-related GBS.

In the present study, C-Dps was found to bind to myelin in the CNS and PNS as well as to neurons in the anterior horns and cerebral cortex similar to the immunohistochemical staining pattern with anti-sulfatide antibody [26]. Indeed, C-Dps binding was efficiently blocked by the presence of sulfatide, but not other gangliosides. We previously demonstrated by ELISA and immunostaining of thin-layer chromatograms that C-Dps bound to only sulfatide among various glycolipids, namely, GM1, GM2, GM3, GD1a, GD1b, GD3, GT1b, GQ1b, galactocerebroside, sufatide and bovine brain ganglioside type III [21]. These findings suggest that C-Dps binds to sulfatide in tissue; however, it is also possible that C-Dps may also bind to other glycolipids or glycoproteins with a similar structure to sulfatide. Interestingly, anti-sulfatide antibodies have been reported to be present in various inflammatory neurological diseases, such as multiple sclerosis [27], dysimmune peripheral neuropathy [28–33] and the distal sensory neuropathy seen in HIV-infected individuals [34]. In patients with dysimmune neuropathy who have anti-sulfatide antibodies, pathological and electrophysiological studies have revealed mostly demyelinating neuropathy with prominent axonal involvement [35, 36]. Anti-sulfatide antibodies have been demonstrated to bind not only central and peripheral myelin, but also dorsal root ganglion cells and neuroblastoma cells [29]. The nodes of Ranvier and Schmidt-Lanterman incisures are stained extensively by anti-sulfatide antibody [37]. Experimental passive transfer of anti-sulfatide antibody caused demyelination of peripheral nerves with deposition of the antibody at the nodes of Ranvier and Schmidt-Lanterman incisures [38]. Interestingly, given that some GBS patients develop CNS symptoms and signs such as hyperreflexia and other pyramidal tract signs and disturbances of consciousness [39], C-Dps may even contribute to such a CNS involvement.

No consensus has emerged regarding the effects of anti-GM1 antibody treatment on myelinated axons in either isolated nerve preparations or following intraneural injection: some authors have reported a conduction block and pathological changes [11, 16, 40, 41], while others have not [14, 42, 43]. Such an inconsistency is considered to be attributable to the GM1 microenvironment in vivo, where GM1 epitopes are embedded and hidden [16]. We thus consider that C-Dps, which preferentially binds to the nodes of Ranvier, may be a candidate neurotoxin produced by *C. jejuni*, and may augment the actions of anti-GM1 antibody via disclosure of hidden GM1 epitopes at the node.

Acknowledgments This work was supported in part by grants from the Ministry of Education, Culture, Sports, Science and Technology of Japan, a Neuroimmunological Disease Research Committee grant from the Ministry of Health, Labour and Welfare of Japan and a grant for Research on Brain Science. We thank Tomo Iwashima and Magnus Hallstrom for their technical assistance.

References

1. Yuki N (2001) Infectious origins of, and molecular mimicry in, Guillain-Barré and Fisher syndromes. Lancet Infect Dis 1:29–37
2. Ho TW, Mishu B, Li CY et al (1995) Guillain-Barré syndrome in northern China: relationship to *Campylobacter jejuni* infection and anti-glycolipid antibodies. Brain 118:597–605
3. McKhann GM, Cornblath DR, Griffin JW et al (1993) Acute motor axonal neuropathy: a frequent cause of acute flaccid paralysis in China. Ann Neurol 33:333–342
4. Griffin JW, Li CY, Ho TW et al (1996) Pathology of the motor-sensory axonal Guillain-Barré syndrome. Ann Neurol 39:17–28
5. Kuwabara S, Ogawara K, Misawa S et al (2004) Does *Campylobacter jejuni* infection elicit"demyelinating"Guillain-Barré syndrome? Neurology 63:529–533
6. Hiraga A, Kuwabara S, Ogawara K et al (2005) Patterns and serial changes in electrodiagnostic abnormalities of axonal Guillain-Barré syndrome. Neurology 64:856–860
7. Griffin JW, Li CY, Ho TW et al (1995) Guillain-Barré syndrome in northern China. The spectrum of neuropathological changes in clinically defined cases. Brain 118:577–595
8. Griffin JW, Li CY, Macko C et al (1996) Early nodal changes in the acute motor axonal neuropathy pattern of the Guillain-Barré syndrome. J Neurocytol 25:33–51
9. Ariga T, Yu RK (2005) Antiglycolipid antibodies in Guillain-Barré syndrome and related diseases: review of clinical features and antibody specificities. J Neurosci Res 80:1–17
10. Hafer-Macko C, Hsieh S-T, Li CY et al (1996) Acute motor axonal neuropathy: an antibody-mediated attack on axolemma. Ann Neurol 40:635–644
11. Susuki K, Rasband MN, Tohyama K et al (2007) Anti-GM1 antibodies cause complement-mediated disruption of sodium channel clusters in peripheral motor nerve fibers. J Neurosci 27:3956–3967
12. Rees JH, Gregson NA, Hughes RA (1995) Anti-ganglioside GM1 antibodies in Guillain-Barré syndrome and their relationship to *Campylobacter jejuni* infection. Ann Neurol 38:809–816
13. Willison HJ, Yuki N (2002) Peripheral neuropathies and anti-glycolipid antibodies. Brain 125:2591–2625
14. Hirota N, Kaji R, Bostock H et al (1997) The physiological effect of anti-GM1 antibodies on saltatory conduction and transmembrane currents in single motor axons. Brain 120:2159–2169
15. Sheikh KA, Zhang G, Gong Y et al (2004) An anti-ganglioside antibody-secreting hybridoma induces neuropathy in mice. Ann Neurol 56:228–239
16. Greenshields KN, Halstead SK, Zitman FMP et al (2009) The neuropathic potential of anti-GM1 autoantibodies is regulated by the local glycolipid environment in mice. J Clin Invset 119:595–610
17. Ishikawa T, Mizunoe Y, Kawabata S et al (2003) The iron-binding protein Dps confers hydrogen peroxide stress resistance to *Campylobacter jejuni*. J Bacteriol 185:1010–1017
18. Teneberg S, Miller-Podraza H, Lampert HC et al (1997) Carbohydrate binding specificity of the neutrophil-activating protein of *Helicobacter pylori*. J Biol Chem 272:19067–19071
19. Honke K, Hirahara Y, Dupree J et al (2002) Paranodal junction formation and spermatogenesis require sulfoglycolipids. Proc Natl Acad Sci USA 99:4227–4232
20. Ishibashi T, Dupree JL, Ikenaka K et al (2002) A myelin galactolipid, sulfatide, is essential for maintenance of ion channels on myelinated axon but not essential for initial cluster formation. J Neurosci 22:6507–6514
21. Piao H, Minohara M, Kawamura N et al (2010) Induction of paranodal myelin detachment and sodium channel loss in vivo by *Campylobacter jejuni* DNA-binding protein from starved cells (C-Dps) in myelinated nerve. J Neurol Sci 288:54–62
22. Toda K, Small JA, Goda S et al (1994) Biochemical and cellular properties of three immortalized Schwann cell lines expressing different levels of the myelin-associated glycoprotein. J Neurochem 63:1646–1657
23. Li S, Liquari P, McKee KK et al (2005) Laminin-sulfatide binding initiates basement membrane assembly and enables receptor signaling in Schwann cells and fibroblasts. J Cell Biol 169:179–189
24. Saito F, Moore SA, Barresi R et al (2003) Unique role of dystroglycan in peripheral nerve myelination, nodal structure, and sodium channel stabilization. Neuron 38:747–758
25. Wirguin I, Rosoklija G, Trojaborg W et al (1995) Axonal degeneration accompanied by conduction block induced by toxin mediated immune reactivity to GM1 ganglioside in rat nerves. J Neurol Sci 130:17–21
26. Pernber Z, Molander-Melin M, Berthold CH et al (2002) Expression of the myelin and oligodendrocyte progenitor marker sulfatide in neurons and astrocytes of adult rat brain. J Neurosci Res 69:86–93
27. Ilyas AA, Chen Z-W, Cook SD (2003) Antibodies to sulfatide in cerebrospinal fluid of patients with multiple sclerosis. J Neuroimmunol 139:76–80
28. Pestronk A, Li F, Griffin J et al (1991) Polyneuropathy syndromes associated with serum antibodies to sulfatide and myelin-associated glycoprotein. Neurology 41:357–362
29. Quattrini A, Corbo M, Dhaliwal SK et al (1992) Anti-sulfatide antibodies in neurological disease: binding to rat dorsal root ganglia neurons. J Neurol Sci 112:152–159
30. Nemni R, Fazio R, Quattrini A et al (1993) Antibodies to sulfatide and to chondroitin sulfate C in patients with chronic sensory neuropathy. J Neuroimmunol 43:79–85
31. van den Berg LH, Lankamp CLAM, de Jager AEJ et al (1993) Antisulfatide antibodies in peripheral neuropathy. J Neurol Neurosurg Psychiatry 56:1164–1168
32. Nobile-Orazio E, Manfredini E, Carpo M et al (1994) Frequency and clinical correlates of anti-neural IgM antibodies in neuropathy associated with IgM monoclonal gammopathy. Ann Neurol 36:416–424
33. Isoardo G, Ferrero B, Barbero P et al (2001) Anti-GM1 and anti-sulfatide antibodies in polyneuropathies. Threshold titers and accuracy. Acta Neurol Scand 103:180–187
34. Lopate G, Pestronk A, Evans S et al (2005) Anti-sulfatide antibodies in HIV-infected individuals with sensory neuropathy. Neurology 64:1632–1634
35. Carpo M, Meucchi N, Allaria S et al (2000) Anti-sulfatide IgM antibodies in peripheral neuropathy. J Neurol Sci 176:144–150
36. Erb S, Ferracin F, Fuhr P et al (2000) Polyneuropathy attributes: a comparison between patients with anti-MAG and anti-sulfatide antibodies. J Neurol 247:767–772
37. Petratos S, Turnbull VJ, Papadopoulos R et al (1999) Peripheral nerve binding patterns of anti-sulfatide antibodies in HIV-infected individuals. Neuroreport 10:1659–1664
38. Nardelli E, Bassi A, Mazzi G et al (1995) Systemic passive transfer studies using IgM monoclonal antibodies to sulfatide. J Neuroimmunol 63:29–37
39. Kuwabara S, Nakata M, Sung J-Y et al (2002) Hyperreflexia axonal Guillain-Barré syndrome subsequent to *Campylobacter jejuni* enteritis. J Neurol Sci 199:89–92

40. Willison HJ, O'Hanlon G, Paterson G et al (1997) Mechanisms of action of anti-GM_1 and anti-GQ_{1b} ganglioside antibodies in Guillain-Barré syndrome. J Infect Dis 176:S144–S149
41. Takigawa T, Yasuda H, Kikkawa R et al (1995) Antibodies against GM_1 ganglioside affect K^+ and Na^+ currents in isolated rat myelinated nerve fibers. Ann Neurol 37:436–442
42. Buchwald B, Toyka KV, Zielasek J et al (1998) Neuromuscular blockade by IgG antibodies from patients with Guillain-Barré syndrome: a macro-patch-clamp study. Ann Neurol 44:913–922
43. Dilley A, Gregson NA, Hadden RDM et al (2003) Effects on axonal conduction of anti-ganglioside sera and sera from patients with Guillain-Barré syndrome. J Neuroimmunol 139:133–140

Journal of the Neurological Sciences 297 (2010) 89–91

Contents lists available at ScienceDirect

Journal of the Neurological Sciences

journal homepage: www.elsevier.com/locate/jns

Short Communication

Recurrent Hopkin's syndrome: A case report and review of the literature

Pavone Piero [a,*], Maria Roberta Longo [a], Ferdinando Scalia [a], Riccardo Polosa [b], Jun-ichi Kira [c], Raffaele Falsaperla [a]

[a] Department of Pediatric and Pediatric Neurology, Azienda Ospedaliera Universitaria OVE-Policlinico, Università di Catania, Catania, Italy
[b] Department of Internal Medicine, Azienda Ospedaliera Universitaria OVE-Policlinico, Università di Catania, Catania, Italy
[c] Department of Neurology, Neurological Institute, Graduate School of Medical Sciences, Kyushu University, Fukuoka, 812-8582, Japan

ARTICLE INFO

Article history:
Received 2 March 2010
Received in revised form 30 June 2010
Accepted 13 July 2010
Available online 7 August 2010

Keywords:
Hopkin's syndrome
Atopy
Atopic myelitis
Recurrence
IgE

ABSTRACT

Flaccid paralysis affecting one or more limbs after an asthma attack is a poliomyelitis-like illness known as Hopkins' syndrome (HS). Although a viral infection or multifactorial immune suppression during an acute attack of bronchial asthma has been proposed to be the mechanism involved in this syndrome, the precise etiopathogenetic mechanism remains unknown. We report a 13-year-old girl who had recurrent acute episodes of myelitis after asthma attacks. She had four episodes of acute flaccid paralysis, each of which was preceded by acute asthma attacks. Some of the attacks were accompanied by sensory and sphincter disturbances. She had hyperIgEaemia and the prick test to *Dermatophagoides farinae* and cedar pollen was strongly positive. The present case is the first HS case demonstrating frequent recurrences and suggests a possible link between HS and atopic myelitis.

1. Introduction

Hopkins syndrome (HS; asthmatic amyotrophy) is a rare disease involving the anterior horn cells following an acute asthma attack [1–4]. This condition usually affects children with atopic asthma. Typically, several days to a few weeks after an asthma attack, affected children exhibit the acute onset of flaccid paralysis involving one or two limbs, subsequently progressing to severe muscle atrophy of the affected limb [5]. There is a poor response to corticosteroids in most cases, which do not usually recur [6]. We report a 13-year-old girl who had recurrent episodes of HS.

2. Case presentation

G. L. is a 13-year-old girl with a history of bronchitis asthmatiform since 2 years of age and bronchial asthma since 9 years of age. At that time, she had a complete blood count within the normal range and a serum IgE value of 128 U/ml, even though the prick test showed marked reactions to *Dermatophagoides farina* and cedar pollen. After that episode, she had been receiving inhalation therapy with beta agonists and montelukast sodium. The girl came to our attention during another asthma attack consisting of dyspnea (SaO_2, 90%), wheezing, cough, and tachypnea. At the time of admission, she had no fevers and a respiratory rate of 32 per min. Bilateral expiratory wheezes and scattered rhonchi in the lower lobes were present. A thoracic X-ray was normal. Her complete blood count was as follows: 10,300 white cells/mm^3, with 55% neutrophils, 7.5% eosinophils, 32.5% lymphocytes, and 5.0% monocytes. The other routine laboratory tests were normal. She underwent oral erythromycin and aereosol therapy, including adrenaline, with an improvement in the respiratory symptoms in 2 days. Five days after the acute asthma attack, sensorimotor disturbances in both legs were noticed. Headaches, vertigo, severe muscle weakness, and difficulty in ambulation appeared over the next 2 days. The neurologic examination revealed severe hypotonia in both lower limbs. The deep tendon reflexes of the lower limbs were normal. The days later the deep tendon reflexes showed lower limb hyperreflexia. She presented with progressive deterioration in her clinical condition with loss of sensibility below both knees, rachialgy, and an alteration in sphincter tone. The anti-viral antibodies in paired serum samples showed no significant changes in any viruses examined, including herpes 1 and 2, echovirus, enterovirus, coxsackievirus, and poliovirus types 1, 2, and 3. TORCH, anti-mycoplasma, and anti-borrelia titers were normal. Anti-cardiolipin, anti-phospholipin, anti-cytoplasmatic, anti-nuclear, anti-DNA, and anti-myelin antibodies were absent.

Serum and urinary amino acids, serum ammonia, and blood lactic acid levels were also normal. A CSF examination showed 120 mononuclear cells/ml, protein at 50 mg/dl, an increase in the IgG index (0.8), and negative oligoclonal bands. The cerebrospinal fluid cultures were negative. The serum IgE was elevated (558 U/ml). No cardiac abnormalities were noted on clinical and ultrasound

* Corresponding author. UO Pediatria, Azienda Ospedaliera Universitaria, OVE-Policlinico, Via Plebiscito 759, Catania, Italy. Tel.: +39 095 3782682; fax: +39 095 222532.
E-mail address: ppavone@unict.it (P. Piero).

0022-510X/$ – see front matter © 2010 Elsevier B.V. All rights reserved.
doi:10.1016/j.jns.2010.07.005

examinations. The EEG was characterized by diffuse slow waves. Abdominal ultrasound and CT scans were normal.

A needle EMG did not show any abnormalities and the motor nerve conduction velocity (MCV) within the normal range. F waves were evoked in all nerves. The sensory nerve conduction velocity (SCV) was also normal. The somatosensory evoked potential (SEPs) in the legs were all normal. A brain MRI was normal. Intravenous IgG was started at a dose of 1 g/kg/day for 3 days.

Methylprednisolone pulse therapy was initiated (1000 mg/day for 4 days), followed by oral corticosteroids (50 mg/day) with gradual tapering. The therapy, including corticosteroids, alleviated her sensory impairment, but had no effect on the muscle weakness. Rehabilitation was initiated for 3 months for the residual motor impairment.

After 3 months, she developed another attack similar to the one previously described (7 days after the acute asthma attack), and sensorimotor disturbances in both legs were noticed. Headaches, vertigo, moderate muscle weakness, and difficulty in ambulation were less severe than the former attack. Methylprednisolone pulse therapy was initiated, with an improvement in her general condition, followed by oral corticosteroids with gradual tapering. During corticosteroid therapy, she experienced another asthma attack, and 6 days later she developed right arm weakness. Upper muscles had mild-to-moderate weakness. Deep tendon reflexes were depressed in both upper limbs. Pathologic reflexes were negative. Hypesthesias, paresthesias, and hypalgesias were present in the left C5-6 and C7 dermatomes. No sphincter disturbance was noted.

The total white blood count was 11,000/mm^3, with 55.6% neutrophils, 6% eosinophils, 34.4% lymphocytes, and 5.0% monocytes. The serum IgE was increased (996 U/ml). A cervical MRI was unchanged with respect to the first episode. Moderate weakness in the right arm remained despite corticosteroid therapy.

Two years later she experienced a new episode, after another asthma attack, and 3 days later she developed right and left arm weakness. Muscles upper limbs had mild-to-moderate weakness. Deep tendon reflexes were depressed in both upper limbs. The pathologic reflexes were negative. Hypesthesias, paresthesias, and hypalgesias were present in the left C5-6 and C7 dermatomes. A mild hypotrophia of both legs was noticed. No sphincter disturbances were noted. The total white blood count was 15,000/mm^3, with 44.8% neutrophils, 9% eosinophils, 44.2% lymphocytes, and 3.0% monocytes. The serum IgE was increased (822 U/ml). The brain MRI, including the cervical spinal cord and brachial plexus, was normal. During a 5-year follow-up from the first episode there were no new clinical symptoms.

3. Discussion

HS is a rare disease involving anterior horn cells following an acute asthma attack, most often in children that have atopic asthma [1–6]. In general, this disease occurs from several days to a few weeks after an acute attack of asthma, manifesting as the acute onset of flaccid paralysis of one or both limbs, and progressing in most cases to severe muscle atrophy of the affected limb [3–5]. In such episodes, there is a poor response to corticosteroids and usually there are no recurrences [6]. However, some cases have predominant ventral root involvement [8], while other cases exhibit an extension of the lesions into the anterior columns on MRI [9,10]. Thus, the site of lesions in HS is not strictly limited to the anterior horn. It is reported that patients with asthma demonstrate more cytokine production from peripheral blood lymphocytes on stimulation with allergens than those with skin allergy [11], but currently there is no evidence-based clinical correlation between cytokine production and HS.

A clinical entity with similarity to HS is atopic myelitis (AM). Many reports have confirmed the evidence in the central nervous system (CNS) or peripheral nervous system (PNS) in patients with high level of total Ig E [7] and co-existing atopic disease. AM is a myelitis of unknown cause that occurs in patients with longstanding atopic disorders, such as atopic dermatitis and airway allergy [10–13]. The disease preferentially affects the posterior column of the cervical spinal cord, thus predominantly presenting paresthesias/dysesthesias in the distal parts of the four limbs [10–14]. HS and AM differ from each other in the preferential age of onset, neurologic manifestations, and preferential sites of spinal cord involvement. However, both conditions are similar regarding the most important point that myelitis develops in the presence of atopic disorders, which suggests a link between atopy and the development of spinal cord inflammation. In 2008, Kira et al. [10] described 22 patients with myelitis of unknown etiology and atopic diathesis, 5 of whom showed focal amyotrophy in one or two limbs. A possible link was postulated between AM and HS. AM and HS could be an allergic mechanism due cross reactivity between an allergen and CNS or PNS.

Our patients developed brain involvement represented by headache, vertigo and EEG abnormalities and flaccid paralysis without amyotrophy and several recurrences, with a close temporal relation to an acute asthma attack. Our patient fits well into this category (HS or AM). Horiuchi et al. [15] described a 22-year-old woman who showed an additional episode of myelitis after another asthma attack, although no relapse has ever been reported in cases of HS [1–15] (Table 1). This is the first report describing the occurrence of recurrent asthmatic flaccid paralysis in childhood. Since our patient had hyperIgEaemia and allergen-specific IgE, the bronchial asthma seen in our patients was most likely atopic. HyperIgEaemia and allergen-specific IgE were also found in reported cases of HS [9–13]. As a result, the preceding asthma in HS is also considered to be atopic. It has been postulated that latently infected polioviruses within the anterior horn cells are activated under non-specific immunosuppressed conditions induced by bronchial asthma, thereby destroying the infected cells in HS [16]. However, no increase in anti-poliovirus antibodies has been detected in this condition, including our patient. As our case demonstrated myelitis was recurrent and each episode tightly associated with asthma attacks and symptoms possibly caused by lesions affecting nerve root.

The present case strongly suggests a possible link between HS and AM. AM and HS could represent the same entity with different clinical pictures based on different areas of involvement of the CNS and PNS.

As the number of adult and young patients with atopic disorders is greatly increasing in many industrialised countries, further studies

Table 1
Clinical data of our patient with recurrent Hopkins syndrome versus the literature.

	Our patient	Patient 2 of Horiuchi et al.
Age at onset/gender	13/Female	22/Female
Serum total IgE (U/ml)	558 (2′ 996)	298
Eosinophils (%)	7.5%	6.5%
Interval between asthma attacks and onset of myelitis (days)	5 (1′) and 7 (2′) 6(3′) 3(4′)	7 (1′) and 9 (2′)
Symptoms and signs during illness		
Motor weakness	+ + (bilateral)	+ (monoparesis)
Muscle atrophy	±	+
Increased tendon reflex 6 days	+++	+ (2′)
Sensory signs	±(1′) ++ (2′)	+
Sphincter disturbance	+ only in 1st episode	absent
CSF		
Increased protein (>45 mg/dl)	50	52
Clinical course	Improved	Slightly improved

*Our patient had 4 episodes; Patient 2 (Horiuchi) had 2 recurrent episodes.
1′ = the first episode; 2′ = the second episode; 3′ = the third episode; 4′ = the fourth episode.

need to be done to better clarify the relationship between asthma and myelitis.

Acknowledgements

We are grateful to Prof. Lorenzo Pavone for the helpful suggestions and the critical review of the manuscript. We also wish to thank Prof. R. Trifiletti and the International Science Editing Co. (Shannon Ireland) for editing the manuscript.

References

[1] Blomquist HKS, Bjorkstin B. Poliomyelitis-like illness associated with asthma. Arch Dis Child 1980;55:61–3.
[2] Hopkins IJ. A new syndrome: poliomyelitis-like illness associated with acute asthma in childhood. Aust Paediatr J 1974;10:273–6.
[3] Ilett SJ, Pugh RJ, Smithells RW. Poliomyelitis-like illness after acute asthma. Arch Dis Child 1977;52:738–40.
[4] Shapiro GG, Chapman JT, Pierson WE, Bierman CW. Poliomyelitis like illness after acute asthma. J Pediatr 1979;94:767–8.
[5] Hopkins IJ, Shield LK. Poliomyelitis-like illness associated with asthma in childhood. Lancet 1974;1:760.
[6] Shahar EM, Hwang PA, Niesen CE, Murphy EG. Poliomyelitis-like paralysis during recovery from acute bronchial asthma: possible etiology and risk factors. Pediatrics 1991;88:276–9.
[7] Osoegawa M, Ochi H, Yamada T, Horiuchi I, Murai H, Furuya H, et al. High incidence of subclinical peripheral neuropathy in myelitis with hyperIgEaemia and mite antigen-specific IgE (atopic myelitis): an electrophysiological study. Intern Med 2002;41:684–91.
[8] Danta G. Electrophysiological study of amyotrophy associated with acute asthma (asthmatic amyotrophy). J Neurol Neurosurg Psychiatry 1975;38:1016–21.
[9] Liedholm LJA, Eeg-Olofsson O, Ekenberg BEK, Nicolaysen RB, Torbergsen T. Acute postasthmatic amyotrophy (Hopkins' syndrome). Muscle Nerve 1994;17:769–72.
[10] Kira J, Isobe N, Kawano Y, Osoegawa M, Ohyagi Y, Mihara F, et al. Atopic mielitis with focal amyotrophy: a possible link to Hopkins syndrome. J Neurol Sci 2008;269(1–2):143–51.
[11] Kimura M, Tsuruta S, Yoshida T. Differences in cytokine production by peripheral blood mononuclear cells (PBMC) between patients with atopic dermatitis and bronchial asthma. Clin Exp Immunol 1999;118:192–6.
[12] Kira J, Yamasaki K, Kawano Y, Kobayashi T. Acute myelitis associated with hyperIgEemia and atopic dermatitis. J Neurol Sci 1997;148:199–203.
[13] Kira J, Kawano Y, Yamasaki K, Tobimatsu S. Acute myelitis with hyperIgEaemia and mite antigen specific IgE: atopic myelitis. J Neurol Neurosurg Psychiatry 1998;64:676–9.
[14] Kira J, Kawano Y, Horiuchi I, Yamada T, Imayama S, Furue M, et al. Clinical, immunological and MRI features of myelitis with atopic dermatitis (atopic myelitis). J Neurol Sci 1999;162:56–61.
[15] Horiuchi I, Yamasaki K, Osoegawa M, Ohyagi Y, Okayama A, Kurokawa T, et al. Acute myelitis after asthma attacks with onset after puberty. J Neurol Neurosurg Psychiatry 2000;68:665–8.
[16] Manson JI, Thong YH. Immunological abnormalities in the syndrome of poliomyelitis-like illness associated with acute bronchial asthma (Hopkins' syndrome). Arch Dis Child 1980;55:26–32.

Acta Neuropathol (2010) 120:651–660
DOI 10.1007/s00401-010-0733-7

ORIGINAL PAPER

Aquaporin-4 astrocytopathy in Baló's disease

Takeshi Matsuoka · Satoshi O. Suzuki · Toru Iwaki · Takeshi Tabira · Artemio T. Ordinario · Jun-ichi Kira

Received: 11 June 2010 / Revised: 22 July 2010 / Accepted: 27 July 2010 / Published online: 3 August 2010

Abstract Baló's concentric sclerosis (BCS) is considered to be a rare variant of multiple sclerosis and characterized by alternating rings of demyelinated and preserved myelin layers. The mechanism underlying BCS remains to be elucidated. Recently, occurrence of concentric rings of Baló was described in the brainstem of a patient with neuromyelitis optica (NMO). Because selective loss of aquaporin-4 (AQP4) and vasculocentric deposition of complement and immunoglobulins are characteristic in NMO, we aimed to assess AQP4 expression in the concentric demyelinating lesions of BCS patients. We evaluated AQP4 expression relative to expression of another astrocytic marker (glial fibrillary acidic protein), the extent of demyelination, lesion staging and perivascular deposition of complement and immunoglobulin in four cases with BCS, and 30 individuals with other neurological diseases. All cases with BCS demonstrated extensive AQP4 loss in both demyelinated and myelinated layers of all actively demyelinating lesions, with perivascular lymphocytic cuffing of T cells, but no deposition of immunoglobulins or complement around vessels. These findings suggest that AQP4 loss occurs in heterogeneous demyelinating conditions, namely NMO and BCS. Furthermore, acute BCS lesions are characterized by extensive AQP4 loss without vasculocentric deposition of complement or immunoglobulin.

Keywords Aquaporin-4 · Astrocyte · Baló's concentric sclerosis · Multiple sclerosis · Neuromyelitis optica

T. Matsuoka · S. O. Suzuki (✉) · T. Iwaki
Department of Neuropathology, Graduate School of Medical Sciences, Kyushu University, 3-1-1 Maidashi, Higashi-ku, Fukuoka 812-8582, Japan
e-mail: sosuzuki@np.med.kyushu-u.ac.jp

T. Matsuoka · J. Kira
Department of Neurology, Graduate School of Medical Sciences, Kyushu University, 3-1-1 Maidashi, Higashi-ku, Fukuoka 812-8582, Japan

T. Tabira
Department of Diagnosis, Prevention and Treatment of Dementia, Graduate School of Juntendo University, 2-11-5 Hongo, Bunkyo-ku, Tokyo 113-0033, Japan

A. T. Ordinario
Department of Neurology and Psychiatry, University of Santo Tomas, Espana Boulevard, Sampaloc, Luzon Manila 1008, Philippines

Introduction

Baló's concentric sclerosis (BCS), a rare variant of multiple sclerosis (MS), was first described by Baló in 1928 [2]. The initial terminology for this entity was encephalitis periaxialis concentrica, which is based on its early definition of "a disease in the course of which the white matter of the brain is destroyed in concentric layers in a manner that leaves the axis cylinders intact" [2]. This condition is relatively frequently reported in some Asian populations including Filipinos [15], southern Han Chinese [38], and Taiwanese [6]. The clinical course is characterized by an acute onset and steady progression to major disability within a few months. It is pathologically characterized by huge, tumor-like brain lesions showing concentric rings of alternating demyelination and preserved myelin layers [7]. Immunohistochemical analysis of ten cases with BCS suggested that this peculiar concentric pattern formation might be attributable to hypoxia-like tissue preconditioning [34]; however, the primary mechanisms that initiate the lesions remain unknown.

On the other hand, neuromyelitis optica (NMO), another demyelinating disorder, also demonstrating extensive lesions in the spinal cord and optic nerves, is thought to be a variant of MS; however, the recent discovery of a specific immunoglobulin G (IgG) against NMO, designated NMO-IgG [20], suggests that NMO is distinct from MS. This IgG targets the aquaporin-4 (AQP4) water channel protein [19], which is strongly expressed on astrocyte foot processes at the blood–brain barrier (BBB) [12]. Autopsied NMO cases show a loss of AQP4 immunostaining in inflammatory lesions, whereas AQP4 expression is increased in the demyelinating plaques in MS patients [27, 30]. The vasculocentric deposition of complement and immunoglobulins in NMO lesions [23] suggests a humoral immune attack against AQP4 on astrocytes, especially as the NMO-IgG/anti-AQP4 antibody is cytotoxic to astrocytes in vitro and in vivo in the presence of complement [3, 4, 13, 14, 31, 32, 36].

Interestingly, Graber et al. [11] recently reported an occurrence of concentric rings of Baló in the brainstem in an Afro-Caribbean patient with NMO. Because AQP4 status has never been studied in BCS, we performed a systematic immunohistological analysis of AQP4 expression in BCS lesions relative to unaffected white matter areas in the same section, astrocyte marker expression, the extent of demyelination, lesion staging and the perivascular deposition of complement and immunoglobulin in four autopsied cases with BCS. All cases showed loss of AQP4 staining but no perivascular deposition of complement or immunoglobulin in the active concentric lesions, suggesting an occurrence of AQP4-related astrocytopathy also in BCS.

Materials and methods

Autopsy cases of BCS and other neurological disorders

This study was performed on archival autopsy brain materials of six concentric demyelinating lesions from four Filipino cases pathologically diagnosed as BCS. The clinical findings of the patients are summarized in Table 1. The cases consisted of two females and two males, and age at autopsy ranged from 23 to 49 years. Disease durations ranged from 0.1 to 0.6 years (median, 0.4 years). In addition, cases with myasthenia gravis (MG) ($n = 2$), spastic paraplegia (SPG) type 2 ($n = 1$), amyotrophic lateral sclerosis (ALS) ($n = 6$), hippocampal sclerosis with temporal lobe epilepsy ($n = 5$), muscular dystrophy ($n = 1$), encephalitis ($n = 3$), including one with anti-*N*-methyl-D-aspartate receptor antibody and another with anti-thyroglobulin antibody, spinocerebellar atrophy (SCA) ($n = 1$), vasculitis ($n = 3$), cerebral infarction ($n = 1$), Pick's disease ($n = 1$), progressive supranuclear palsy ($n = 3$) and multiple system atrophy ($n = 3$) were examined as controls.

Tissue preparation and immunohistochemistry

Autopsy specimens were fixed in 10% buffered formalin and processed into paraffin sections. Sections were routinely stained with hematoxylin and eosin (H&E), Klüver–Barrera (KB) and Bodian or Bielschowsky silver impregnation. The following primary antibodies for immunohistochemistry and staining conditions were used: polyclonal rabbit anti-AQP4 (1:500; Santa Cruz Biotechnology, CA, USA), polyclonal rabbit anti-C3d (1:1000; Dako Cytomation, Glostrup, Denmark), monoclonal mouse anti-C9neo (1:1000; Abcam plc, Cambridge, UK), monoclonal mouse anti-CD68 (1:200; Dako Cytomation, Glostrup, Denmark), monoclonal mouse anti-phosphorylated neurofilament (1:200; Dako Cytomation, Glostrup, Denmark), polyclonal rabbit anti-GFAP (1:1000; Dako Cytomation, Glostrup, Denmark), polyclonal rabbit anti-IgG (1:10000; Dako Cytomation, Glostrup, Denmark), polyclonal rabbit anti-IgM (1:10000; Dako Cytomation, Glostrup, Denmark), monoclonal mouse anti-CD45RO (1:200; Dako Cytomation, Glostrup, Denmark) and monoclonal mouse anti-CD20 (1:200; Dako Cytomation, Glostrup, Denmark). All sections were deparaffinized in xylene and rehydrated in an ethanol gradient. Endogenous peroxidase activity was blocked with 0.3% H_2O_2/methanol. Antigen retrieval was performed by autoclaving sections in 10 mM citrate buffer pH 6.0 before all antibody incubations except for those against AQP4 and GFAP. The sections were then incubated with primary antibody at 4°C overnight. After rinsing, the sections were subjected to either a streptavidin–biotin complex method or an enhanced indirect immunoperoxidase method using Envision (Dako Cytomation, Glostrup, Denmark). Immunoreactivity was detected using 3,3′-diaminobenzidine and sections were counterstained with hematoxylin. Immunohistochemistry for activated complement, immunoglobulins, T cell and B cell markers was performed on randomly selected lesions.

Staging of demyelinating lesions

We classified demyelinating lesions into the following three stages: actively demyelinating lesions, chronic active lesions and chronic inactive lesions based on the density of macrophages phagocytizing myelin debris [16]. Briefly, actively demyelinating lesions were active destructive lesions densely and diffusely infiltrated with macrophages phagocytizing myelin debris, as identified by Luxol fast blue staining. Chronic active lesions were those showing hypercellularity of macrophages restricted to the periphery of the lesions. Chronic inactive lesions were those showing no increase in the numbers of macrophages throughout the

Table 1 Summary of the clinical and pathological findings of cases with Baló's concentric sclerosis

Autopsy	Age (years)	Sex	Disease duration (years)	Relapse rate	Clinically estimated sites of lesions	Pathologically determined sites of lesions
Baló-1	49	M	0.1	NA	Cr (2)[a]	Cr
Baló-2	23	M	0.5	NA	Cr (1)	Cr
Baló-3	28	F	0.3	NA	Cr (1)	Cr
Baló-4	40	F	0.6	NA	Cr (2)	Cr

Cr cerebrum

[a] Number of lesions in parenthesis

lesions. According to the protocol, the six concentric lesions studied were all staged to actively demyelinating lesions.

Comparison of AQP4 expression with myelin loss and astrogliosis

For each lesion, we compared the level of AQP4 expression with the spatial distribution of myelin loss. AQP4 expression levels in region-matched unaffected areas (i.e. gray vs. white mater) in the same section were used as an internal control. To exclude seeming AQP4 down-regulation due to the total loss of astrocytes in such lesions as cavity formation and those totally replaced by macrophages, and to strictly evaluate the AQP4 expression status in the preserved astrocytes in and around the lesions, we confirmed the existence of astrocytes by GFAP staining of neighboring sections for all lesions.

Results

Immunohistochemical findings in control brains

AQP4 expression in pathologically normal brains

AQP4 in normal cerebral tissues from an MG case was diffusely expressed in the cortex, staining the fine processes of the cortical astrocytes (Fig. 1a). Astrocytic perivascular foot processes were more strongly stained with AQP4 than the background neuropil in the cortical gray matter (Fig. 1b, arrows). The glial limiting membranes and subependymal astrocytes also strongly expressed AQP4 (Fig. 1a). There was less AQP4 staining in the white matter than in the cortex, with staining primarily in the perivascular foot processes (Fig. 1c, arrows). In contrast, GFAP immunoreactivity was preferentially observed in the cerebral white matter (Fig. 1d, e). In the cortex, except for the strong staining of the glial limiting membranes (Fig. 1d, arrow), only a few astrocytes were immunopositive for GFAP, with less staining in the perivascular foot processes (Fig. 1f, arrows).

In the cerebellar cortex, both GFAP and AQP4 were expressed in Bergmann glia with radial cytoplasmic processes (Fig. 1g, h), although AQP4 immunoreactivity was generally weaker than that for GFAP. The glial limiting membranes of the cerebellum also strongly expressed GFAP as well as AQP4. In the cerebellar white matter, AQP4 immunoreactivity was mainly observed in the perivascular foot processes, as seen in the cerebral white matter (data not shown).

AQP4 expression in areas of astrogliosis

The normal expression pattern for AQP4 expression was different from that for GFAP as described. However, areas of astrogliosis were generally immunopositive for AQP4 as well as GFAP, in both the gray matter and white matter, regardless of disease types (Fig. 2). For example, hypertrophic gemistocytes in cases of limbic encephalitis (Fig. 2a, b), cerebral infarction (Fig. 2c, d) and SPG type 2 (Fig. 2e, f) showed surface staining for AQP4 in the cytoplasm and processes. Fibrillary gliosis or gliotic scars also showed diffuse AQP4 staining along the glial fibers in cases of SPG type 2 (Fig. 2g, h) and hippocampal sclerosis (data not shown).

Deposition of immunoglobulins and activated complement

Immunohistochemistry for immunoglobulins and activated complement in cerebral tissues from cases with MG, ALS, SCA, vasculitis, limbic encephalitis and cerebral infarction demonstrated weak, diffuse IgG immunoreactivity in the neuronal soma, neuropil, oligodendrocytes, astrocytes, glial limiting membranes and ependymal epithelium, but not in the white matter (data not shown). IgM, C3d and C9neo immunoreactivities were only focally detected in the control cases, and whenever present they were generally confined to blood vessel walls and perivascular regions. Activated complement was not usually co-localized with immunoglobulins; however, in 4 of the 17 cases with non-inflammatory diseases (one each with ALS, SCA, progressive supranuclear palsy and multiple system atrophy) and two of the six cases with inflammatory disorders (anti-*N*-methyl-D-aspartate receptor antibody-seropositive limbic encephalitis and anti-thyroglobulin antibody-seropositive encephalitis), focal perivascular staining for both C3d and IgM was occasionally observed (Fig. 2i, j). In the lesions of patients with ischemic infarction, foamy macrophages were

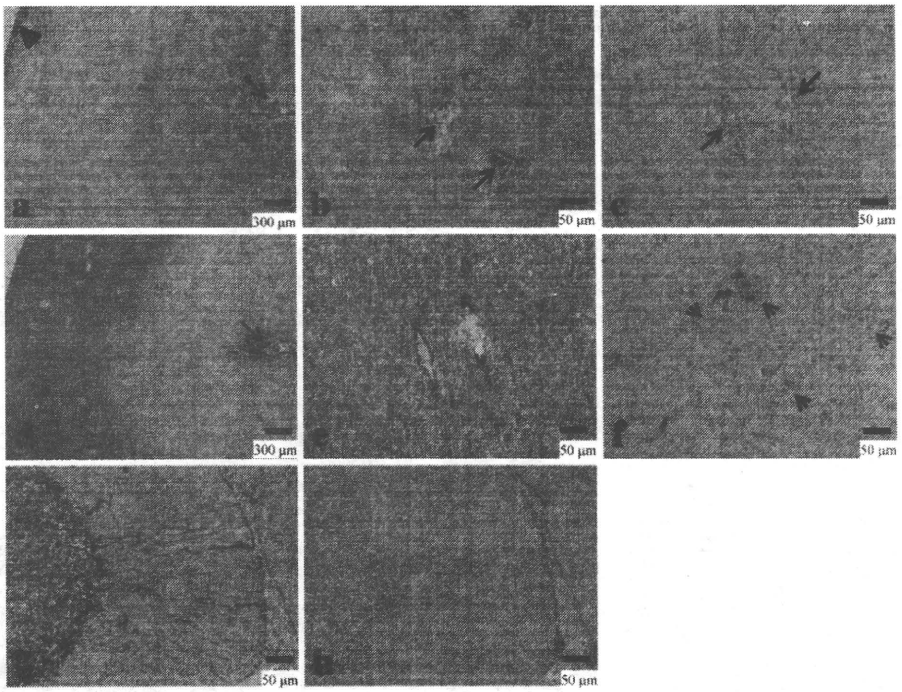

Fig. 1 AQP4 and GFAP expression in normal control brains. A case of MG. AQP4 immunoreactivity is most intense in the glial limiting membrane (*arrow*) and the subependymal astrocytes (*arrowhead*) in the cerebrum. AQP4 is diffusely expressed in the cortex with neuropil staining, while the white matter shows only weak staining (**a**). Higher magnification of the cortex shows strong AQP4 expression in the perivascular foot processes of the cortical astrocytes (*arrows*) (**b**). Higher magnification of the white matter demonstrates an AQP4 staining mainly in the perivascular foot processes of the astrocytes (*arrows*) (**c**). GFAP immunoreactivity is stronger in the white matter than in the cortex. The glial limiting membrane also stains for GFAP (*arrow*) (**d**). Higher magnification of the white matter shows strong GFAP immunoreactivity (**e**). Higher magnification of the cortex shows only scattered GFAP immunoreactive cortical astrocytes and faint staining in the vascular foot processes of astrocytes (*arrows*) (**f**). In the cerebellar cortex, GFAP stains Bergmann glia with radial cytoplasmic processes (**g**). In the cerebellar cortex, AQP4 immunoreactivity is observed in Bergmann glia with radial cytoplasmic processes (**h**). AQP4 (**a–c**, **h**) and GFAP (**d–g**) immunohistochemistry. *Scale bar* 300 μm (**a**, **d**), 50 μm (**b**, **c**, **e–h**), *AQP4* aquaporin-4, *GFAP* glial fibrillary acidic protein, *MG* myasthenia gravis

commonly stained for C3d, C9neo, IgM and IgG. In addition, surface staining of reactive astrocytes was seen with IgG immunostaining, probably due to diffusion of the serum in the affected brain tissue (Fig. 2k–n).

Immunohistochemical findings in BCS

All cases with BCS showed concentric rings of alternating demyelination and preserved myelin layers in the cerebral white matter (Fig. 3a, d). The lesion center was entirely covered with GFAP immunostaining. In the centers of all six actively demyelinating lesions, AQP4 staining was markedly diminished, despite the strong GFAP immunoreactivity (Table 2, Fig. 3c, f, g–l) in both gemistocytic astrocytes (Fig. 3h, i) and astrocytic vascular foot processes (Fig. 3k, l) compared with the unaffected white matter regions with preserved myelin staining (Fig. 3j). The myelin staining negative, peripheral layers of the lesions showed marked decreases of both GFAP and AQP4 staining. High-power field inspection revealed that these areas were almost totally replaced by foamy macrophages (Fig. 3m), with only a small number of highly degenerated GFAP-positive astrocytic processes (Fig. 3n) and axon fragments positive for silver staining (Fig. 3o) and phosphorylated neurofilaments (Fig. 3p). Despite the existence of a few GFAP-positive structures, these areas were totally devoid of AQP4 staining (Fig. 3q). In all lesions, perivascular cuffing with lymphocytes was observed (Fig. 3r). There was dense infiltration of foamy macrophages including myelin debris in the demyelinating layers (Fig. 3s). The perivascular infiltrates predominantly consisted of T cells, while vasculocentric deposition of immunoglobulins (IgG and IgM) or activated complement (C3d and C9neo) was never observed in any of the lesions examined (Table 2; Fig. 3t–v).

Discussion

We performed an immunohistopathological study on AQP4 expression in autopsy cases of BCS. Surprisingly, all cases

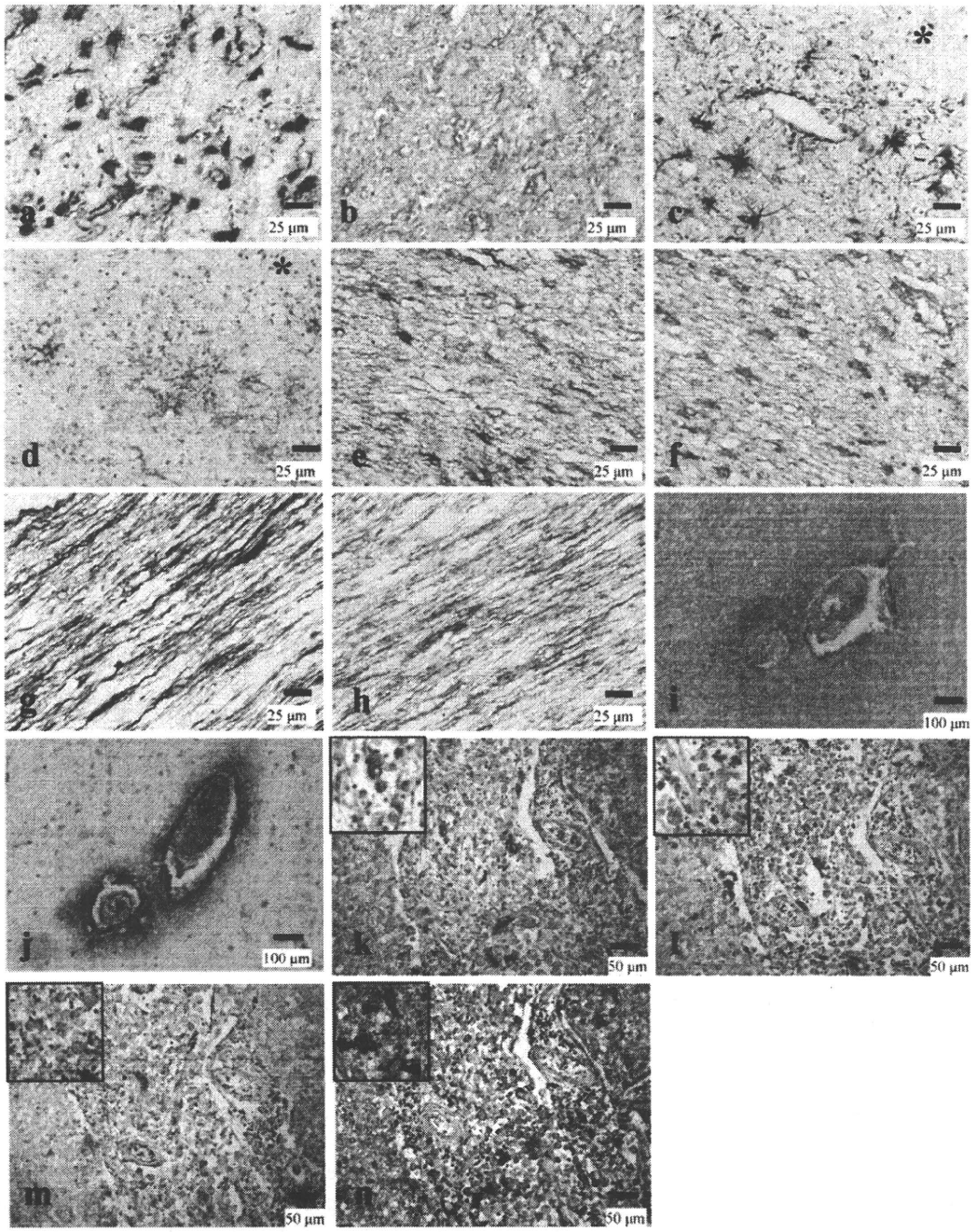

Fig. 2 AQP4, immunoglobulin and complement expression patterns in cases with other neurological diseases. (**a–h**) AQP4 expression in astrogliosis. GFAP-positive gemistocytes (**a**, **c**, **e**) show membranous staining for AQP4 (**b**, **d**, **f**) in cases of limbic encephalitis (**a**, **b**), cerebral infarction (**c**, **d**) and SPG type 2 (**e**, **f**). *Asterisks* in **c** and **d** indicate necrotic areas. Fibrillary gliosis seen in the corpus callosum of the same SPG type 2 case is positive for both GFAP (**g**) and AQP4 (**h**). **i–n** Deposition of immunoglobulins and activated complement (C3d and C9neo) in cases with other neurological diseases. Serial sections distant from focal lesions in the pons from a case with SCA. C3d staining is detected in the perivascular areas (**i**). IgM staining shows a similar pattern to C3d staining (**j**). (**k–n**) Serial sections of the cerebral tissues from a case with cerebral infarction. Numerous macrophages filled with C3d-positive granules in the lesions (*inset* macrophages) (**k**). C9neo staining shows a similar pattern to C3d staining (*inset* macrophages) (**l**). IgM staining shows a similar pattern to activated complement staining (*inset* macrophages) (**m**). IgG staining shows the similar pattern as IgM staining. In addition, staining outlining the cytoplasm of hypertrophic astrocytes was noted (*inset arrowheads*) (**n**). GFAP (**a**, **c**, **e**, **g**), AQP4 (**b**, **d**, **f**, **h**), C3d (**i**, **k**), IgM (**j**, **m**), C9neo (**l**) and IgG (**n**) immunohistochemistry. *Scale bar* 100 μm (**i**, **j**), 50 μm (**k–n**), 25 μm (**a–h**), *AQP4* aquaporin-4, *GFAP* glial fibrillary acidic protein, *SPG* spastic paraplegia, *SCA* spinocerebellar atrophy

with BCS uniformly demonstrated extensive AQP4 loss in all actively demyelinating lesions with perivascular lymphocytic cuffing, but no deposition of immunoglobulins or complement around the blood vessels. Our study indicates that AQP4 loss could occur not only in NMO but also in BCS lesions.

We found a similar AQP4 expression pattern in normal brain tissues to what has been previously reported [27, 30], although we used a different anti-AQP4 antibody to the ones used in those studies. For example, normal cortical astrocytes were diffusely immunostained for AQP4 and weakly immunostained for GFAP, whereas white matter astrocytes showed a reverse pattern. AQP4 is strongly expressed in the glial limiting membranes, and subependymal and perivascular astrocytes. In control diseased brains, both reactive, gemistocytic astrocytes and areas of chronic fibrillary gliosis showed high levels of AQP4 expression regardless of the cause, as previously reported [1, 18, 27, 30]; however, since all the BCS lesions examined in this study were acute lesions, we did not observe chronic fibrillary gliosis and resultant upregulation of AQP4. On the other hand, demyelinating lesions with AQP4 loss generally showed numerous GFAP-immunopositive, gemistocytic astrocytes. In addition, AQP4 expression was lost from GFAP-positive perivascular foot processes. Although some of the myelin-negative foci at the periphery of the concentric lesions showed a decrease in both GFAP and AQP-4 staining, these areas were proven to be necrotic foci with only a small amount of debris from astrocytic processes and axons. Therefore, acute BCS lesions are characterized by AQP4 loss in GFAP-expressing astrocytes and their vascular foot processes, distinct from the staining pattern in NMO in which astrocytes reportedly lose both GFAP and AQP4 staining [27].

This is the first report to show AQP4 loss in BCS cases, not only in the layers showing demyelination, but also in the layers with preserved myelin. All actively demyelinating lesions in BCS showed the same pattern of AQP4 loss, but other acute inflammatory conditions such as limbic encephalitis did not show such AQP4 loss in lesions, suggesting that AQP4 loss is an inherent component of this acute disease. We are currently examining AQP4 status in NMO and MS cases in comparison with that in BCS cases.

All autopsied materials were archival ones taken long before the discovery of NMO-IgG/anti-AQP4 antibody, and the anti-AQP4 antibody statuses of the present BCS cases are unknown. However, because the vasculocentric deposition of complement and immunoglobulins was not confirmed in any of the BCS lesions, an autoantibody and complement-mediated mechanism, which is considered to be unique to NMO, may not be operative in BCS. In future, it will be necessary to measure levels of anti-AQP4 antibody in a large clinical series of BCS patients.

Fig. 3 Representative AQP4 expression pattern in concentric or lamellar demyelinating lesions. Serial sections of the cerebral tissue with actively demyelinating lesions in the white matter from case Baló-1 (**a–c**) and case Baló-2 (**d–s**). The cerebral white matter reveals concentric or lamellar demyelinated lesions (**a**, **d**). GFAP is expressed in the lesion centre, but is largely diminished in the lamellar necrotic foci at the lesion edge (*arrows*) (**a**, **b**, **d**, **e**). AQP4 immunoreactivity is largely lost in the lesion centre with lamellar myelin-staining patterns (**c**, **f**). Numerous reactive, hypertrophic astrocytes are seen in both the demyelinating and preserved myelin layers (**g**). Astrocytes in (**g**) strongly express GFAP (**h**) but lack surface staining for AQP4 (**i**). In the unaffected white matter with preserved myelin staining and no inflammatory infiltration in the same section (the area indicated by *arrowhead* in **d**), non-reactive astrocytes show AQP4 staining on the cell surface and their processes (**j**) and AQP4 expression is also preserved in the perivascular astrocytic foot processes (**k**). In the lesions, however, the perivascular AQP4 staining also disappears (**l**). High-power field views of GFAP-negative necrotic foci at the lesion edge (indicated by *arrows* in **a**, **b**, **d**, **e**) reveal dense infiltration of foamy macrophages (**m**), a small number of highly degenerative, remaining astrocytes (**n**), axons (*arrowheads* in **o**, **p**) and foamy spheroids (*arrows* in **p**). AQP4 immunoreactivity is totally lost in the necrotic areas (**q**). Perivascular accumulation of lymphocytes is noted all over the lesion (**r**). Dense infiltration of foamy macrophages phagocytosing myelin debris in the demyelinating layer (**s**). Perivascular lymphocytes are immunopositive for the T cell marker CD45RO (**t**), but negative for the B cell marker CD20 (**u**). IgG, IgM, C3 and C9neo labeling is detected in some glial cells, but not in the perivascular areas (**v**). Klüver–Barrera staining (**a**, **d**, **s**), hematoxylin and eosin staining (**g**, **m**, **r**), GFAP (**b**, **e**, **h**, **n**) AQP4 (**c**, **f**, **i–l**, **q**), Bielschowsky's silver staining (**o**), phosphorylated neurofilament (**p**), CD45RO (**t**), CD20 (**u**) and IgG, IgM, C3 and C9neo (**v**) immunohistochemistry. *Scale bar* 4 mm (**a–f**), 100 μm (**v**), 50 μm (**k**, **l**, **t**, **u**), 25 μm (**g–j**, **m–s**). *AQP4* aquaporin-4, *GFAP* glial fibrillary acidic protein

The lesions in BCS are classified as type 3 lesions as described by Lucchinetti et al. [22], and the disease is considered to be an oligodendrocytopathy. However, we found AQP4 down-regulation in both demyelinated and myelinated layers, suggesting that astroglial damage occurs more widely than oligodendroglial damage. Hypoxia-like tissue injury may contribute to Baló's lesions [24, 34], which can show restricted diffusion on diffusion-weighted MRI sequences, as happens in acute stroke [39]. Because AQP4 is down-regulated in hypoxic conditions and in the ischemic core at the acute stage [9, 10, 17, 26], vessel obliteration or mitochondrial impairment [24] associated with heavy lymphocytic inflammation may lead to tissue hypoxia and AQP4 down-modulation in BCS.

It has recently been reported that reactive astrocytes that form perivascular scars act as barriers to leukocytes and that conditioned ablation of reactive astrocytes strengthens inflammation [37]. Because AQP4 deletion impairs glial scar formation [35], down-regulation of AQP4 in BCS may enhance inflammatory changes through interruption of perivascular glial scar formation. On the other hand, AQP4 knockout mice show reduced cytotoxic edema following tissue ischemia and hypoxia [25], suggesting that AQP4 down-regulation is protective. Similarly, experimental

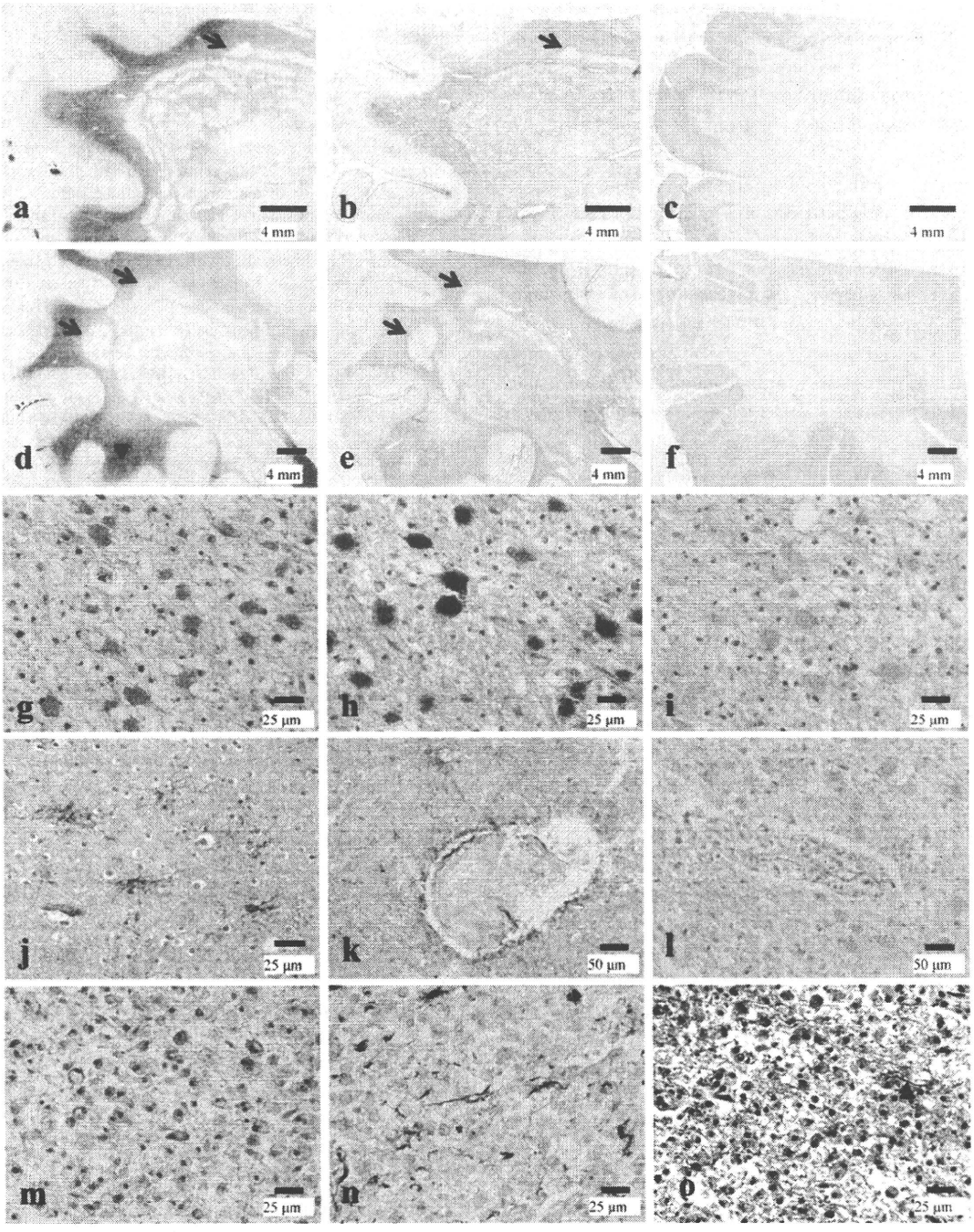

autoimmune encephalomyelitis induced by myelin oligodendrocyte glycoprotein peptide is attenuated in AQP4 knockout mice [21]. These observations suggest that AQP4 down-modulation could be neuroprotective in hypoxia-induced cytotoxic edema as well as in inflammatory demyelinating lesions, which may also be applicable to BCS. On the other hand, it has been reported that AQP4 inhibition causes exacerbation of vasogenic edema [29]. The formation of tumor-like, highly edematous BCS lesions thus might mainly result from vasogenic edema.

In MS, AQP4 loss in actively demyelinating lesions has so far not been reported; Misu et al. [27] found no loss or exaggerated expression of AQP4 in MS plaques, while Roemer et al. [30] detected AQP4 loss in the chronic inactive lesions, suggesting that stage-dependent loss of AQP4 may occur in some MS lesions. Therefore, extensive